Talanta 201 (2019) 465–473

Contents lists available at ScienceDirect

Talanta

journal homepage: www.elsevier.com/locate/talanta

Protein functionalised self assembled monolayer based biosensor for colon cancer detection

Tarun Narayan[a,1], Saurabh Kumar[a,b,1], Suveen Kumar[a,c], Shine Augustine[a], B.K. Yadav[d,e], Bansi D. Malhotra[a,*]

[a] Nanobioelectronics Laboratory, Department of Biotechnology, Delhi Technological University, Delhi, 110042, India
[b] Centre for Nano Science and Engineering (CeNSE), Indian Institute of Science, Bengaluru, 560012, India
[c] Department of Chemistry, University of Delhi, Delhi, 110007, India
[d] Rajiv Gandhi Cancer Institute and Research Centre, Delhi, 110085, India
[e] National Liver Disease Biobank, Institute of Liver and Biliary Sciences, Delhi, 110070 India

ARTICLE INFO

Keywords:
Cancer biomarker
Endothelin-1
Biosensor
Surface plasmon resonance
Electrochemical impedance spectroscopy

ABSTRACT

We report results of the studies relating to the fabrication of a surface plasmon resonance (SPR) based label-free immunosensor for real-time monitoring of endothelin-1 (ET-1), a colon cancer biomarker. A gold disk modified with a self-assembled monolayer (SAM) of 11-mercaptoundecanoic acid (11-MUA) was functionalised via covalent immobilization of monoclonal anti-ET-1 antibodies using EDC-NHS (1-(3-(dimethylamine)-propyl)-3-ethylcarbodiimide hydrochloride, *N*-hydroxy succinimide) chemistry. This immunosensing platform (ethanolamine/anti-ET-1/11-MUA/Au) was characterized via atomic force microscopy (AFM), contact angle (CA) and Fourier transform infrared (FT-IR) spectroscopic techniques. The fabricated SPR electrode was further used to detect ET-1 in the broad concentration range 2–100 pg mL^{-1}, with a detection limit of 0.30 pg mL^{-1} and remarkable sensitivity of 2.18 m^{o} pg^{-1}mL. The adsorption mechanism was studied using monophasic model and the values of association (k_a) and dissociation (k_d) constants for anti-ET-1 and ET-1 binding were calculated to be $4.4 \pm 0.4 \times 10^{5}\ M^{-1}\ s^{-1}$ and $2.04 \pm 0.0003 \times 10^{-3}\ s^{-1}$, respectively. The results obtained via analysis of serum samples of colorectal cancer patients were found to be in good agreement with those obtained from enzyme-linked immunosorbent assay (ELISA) technique. Further, electrochemical studies were performed to prove the efficacy of the fabricated platform as a point of care device for the detection of ET-1.

1. Introduction

Colon cancer, also known as colorectal cancer (CRC), is presently the third most death causing cancer [1]. According to WHO (2012), it is the third most death causing cancer globally [2]. The CRC rates are found to be usually higher in men as compared to women with increased mortality rates in countries having limited resources and inadequate health infrastructure. In India, the five-year survival rates of CRC is less than 40% [3]. CRC usually begins as a non-cancerous polyp that develops on the inner side of the colon and rectum, eventually leading to cancer. The various genetic, environmental and lifestyle-related factors have been reported to contribute to the development of CRC. The environmental and physiological factors that have been observed to affect CRC are age and gender [4], ulcerative colitis [5], long-term immunosuppression [6], diabetes mellitus [7,8], alcohol consumption [9], consumption of red meat [10], obesity [11] and cigarette smoking [12].

The diagnosis of CRC is particularly challenging since the conventional techniques such as physical examination, blood tests [13], colonoscopy [14], histopathology, radiology, and PET-CT scan [15,16] are solely based on evaluation of the symptoms resulting in limited accuracy. Moreover, other techniques, such as biopsy [14], double-contrast barium enema and flexible sigmoidoscopy, depend on the phenotypic properties of the tumor and possess numerous challenges. Despite being sophisticated and selective, these diagnostic techniques are complex, less sensitive, labor-intensive, time-consuming, and have a

Abbreviations: SPRi, Surface plasmon Resonance imaging; LSPR, localized Surface Plasmon Resonance; CA 15-3, Cancer antigen 15-3; GTF2B, General Transcription Factor 2B; ALCAM, Activated leukocyte cell adhesion molecule

* Corresponding author.
E-mail address: bansi.malhotra@gmail.com (B.D. Malhotra).
[1] These authors contributed equally.

https://doi.org/10.1016/j.talanta.2019.04.039
Received 26 February 2019; Received in revised form 12 April 2019; Accepted 15 April 2019
Available online 18 April 2019
0039-9140/

risk of complications like bleeding and bowel tears. Moreover, these methods require advanced instrumentation and well-trained experts for diagnosis. Thus, there is an urgent need to develop an alternative method that is user-friendly, has high throughput screening and is relatively inexpensive for CRC diagnosis.

With the advancement in the stages of CRC, the levels of biomarkers fluctuate indicating state of the disease. Inspection and quantification of these CRC biomarkers can be useful for its timely detection. The biomarkers that are secreted during CRC are carcinoembryonic antigen (CEA) [17], cancer antigen 19-9 (CA 19-9) [18–20], cancer antigen 125 (CA 125), miRNA [21] (miRNA-29a and miRNA-92a), ssDNA [22] (colorectal cancer gene), etc. Among these, CA 19-9 has been found to be less sensitive and is a poor diagnostic marker [23–25]. Moreover, the role of miRNA as a biomarker for CRC detection is not yet well established. The major disadvantage of using ssDNA as a biomarker for cancer detection is that it can be released by the dying tumor cell that remains in circulation as it is highly stable [26]. The challenges posed by these biomarkers open a window for exploring the potential of new markers.

Endothelin-1 (ET-1) is a vasoconstrictor peptide chain of 21 amino acids and can be isolated from endothelial cells [27]. In CRC patients the level of ET-1 in the blood plasma has been found to be elevated in comparison to the normal value [28]. Immunohistochemical analysis of CRC specimens has shown the heterogeneous distribution of ET-1 around tumor cells [29]. Moreover, it is known that ET-1 increases the tumor size when it is added to the growth medium [30–32]. Studies have shown the reported level of ET-1 in serum samples for control subjects to be around $\sim 2.78\ pg\ mL^{-1}$ and in the primary tumor case, it may increase up to $3.9\ pg\ mL^{-1}$. In a patient with metastasis, the ET-1 value rises to $\geq 4.5\ pg\ mL^{-1}$ [33,34]. Many studies have reported that plasma/serum ET-1 concentration rises significantly in the case of CRC [35–37]. Thus, the elevated levels of ET-1 may exhibit a strong correlation with CRC prognosis [28,33,34,38].

The surface plasmon resonance (SPR) is a highly sensitive method that can be used to monitor biomolecular interactions in real-time and can be utilized as a label-free detection for a wide array of molecular interactions, ranging from small ions and viruses to multimolecular complexes [39,40]. The SPR technique allows real-time monitoring of binding kinetics, affinity, specificity, and concentration [41]. Moreover, it also offers fast, label-free detection and is reliable.

We report, for the first time, results of the systematic studies relating to the development of ET-1 immunosensor for detection and real-time monitoring of CRC. Under optimal conditions, the fabricated immunoelectrode exhibited high sensitivity ($2.18\ m^{o}\ pg^{-1}\ mL$) and covered the physiological range of ET-1 biomarker secreted in serum samples of CRC patients. Besides this, we investigated the kinetics of interaction of ET-1 with anti-ET-1 using monophasic model. The immobilization process and binding response were also studied by electrochemical impedance spectroscopy (EIS). The SPR immunosensor exhibited a highly specific interaction between anti-ET-1 and ET-1 biomolecules as compared to other methods. This immunoelectrode was used for the analysis of serum samples from CRC patients and the results showed good correlation with those obtained via the ELISA technique.

2. Materials and reagents

11-mercaptoundecanoic acid, ethanolamine, and 1-(3-(dimethylamine)-propyl)-3-ethylcarbodiimide hydrochloride (EDC), *N*-hydroxysuccinimide (NHS) of AR grade were purchased from Sigma Aldrich, India. Disodium hydrogen phosphate, sodium hydroxide, sodium acetate, potassium chloride (KCl), and polysorbate 20 (tween 20) were procured from Fisher Scientific. Ethanol and acetic acid were purchased from Merck. Sodium dodecyl sulphonate (SDS) was procured from SRL Pvt. Ltd. India. Endothelin-1 (ET-1), and anti-endothelin-1 (monoclonal) were purchased from Biorbyt, USA. 50 nm thick gold-coated BK-7 glass disks (24-mm diameter) were procured from Metrohm Autolab, Netherlands. ET-1 ELISA kit was purchased from Ray Biotech, Inc., India. Patient serum samples were obtained from Rajiv Gandhi Cancer Institute and Research Centre, New Delhi. All experiments were conducted in triplicates (n = 3).

2.1. Preparation of running buffer, regeneration buffer and deactivation solution

Fresh phosphate buffer saline tween (PBST) solution of pH 7.4 was prepared by dissolving salts such as Na_2HPO_4 (0.01 M), NaCl (0.138 M), KCl (0.027 M), and Tween-20 in 200 mL Milli-Q-water. The deactivation solution was prepared using 1 M ethanolamine (pH was adjusted to 8.5 using 1 M HCl) and was used for neutralizing the reactive sites present on the SAM surface. The regeneration buffer was prepared by mixing 10 mM of sodium acetate with 0.1% of SDS (pH was adjusted to 4.5 using acetic acid) and was utilized to remove the analyte present on the surface for re-using the sensor disk. For electrochemical analysis, PBS solution (50 mM, pH 7.4) containing 5 mM $[Fe(CN)_6]^{3-/4-}$ was used. All solutions were prepared in Milli-Q-water (resistivity: 18.2 MΩ cm) and stored at 4 °C.

2.2. Immobilization of anti-ET-1 over the SPR gold disk

Prior to the formation of the desired SAM, the gold (Au) disk was sequentially cleaned with ethanol, acetone and deionized water. Subsequently, the cleaned Au disk was immersed in a solution of 11-MUA (20 mM) in ethanol for 12 h for uniform SAM formation. The strong interaction between the gold and sulfur led to more orderly monolayer formation. The SAM-modified Au Disk (11-MUA/Au) was rinsed with ethanol to remove the unbound 11-MUA molecules. Further, the monoclonal ET-1 antibodies were immobilized onto the 11-MUA/Au disk using EDC–NHS covalent chemistry. Briefly, the 11-MUA/Au disk was flushed with PBST (pH 7.4) for 120 s to obtain a steady baseline, followed by introducing a mixture (30 μL) of 0.4 M EDC and 0.1 M NHS in the ratio of 1:1 for 900 s at 25 °C for activation of 11-MUA SAM surface. Subsequently, 50 μL of monoclonal anti-ET-1($100\ \mu g\ mL^{-1}$) was added onto the EDC-NHS treated 11-MUA/Au disk for covalent immobilization. The activated 11-MUA SAM was bound to the $-NH_2$ group of the anti-ET-1 via EDC-NHS coupling resulting in the formation of an amide bond (Scheme 1). After this, the deactivated buffer of ethanolamine (EA, pH-8.5) solution was introduced for 300s to the anti-ET-1/11-MUA Au disk to deactivate the unbound active sites on the disk. Finally, 30 μL of regeneration buffer (acetic acid + 0.1% SDS; pH 4.5) was added onto the electrode to regenerate and reuse the surface.

2.3. Characterization

The SPR measurements were carried out on SPR TWINGLE (Autolab, Netherlands) instrument having Kretschman configuration. The contact angle measurements were done using SEO Pheonix 300T goniometer (Korea). The Fourier transform infrared (FT-IR) spectroscopic studies of Au disk, 11-MUA/Au disk, and EA/anti-ET-1/11-MUA/Au disk were carried out using a Shimadzu IR Affinity 1S FTIR spectrophotometer. The surface morphology studies on 11-MUA/Au, and anti-ET-1/11-MUA/Au disk was carried out using atomic force microscope (NT-MDT Spectrum Instruments Ltd). Electrochemical impedance spectroscopy (EIS) studies were conducted on an Autolab Potentiostat/Galvanostat (Metrohm, Netherlands) using a three-electrode cell with the modified gold electrode as a working electrode, Ag/AgCl as the reference electrode and platinum as the counter electrode in phosphate buffer saline (PBS, 50 mM, pH 7.4) containing $Fe(CN)_6^{3-/4-}$. The enzyme-linked immunosorbent assay (ELISA) for quantification of ET-1 concentration in the serum samples was conducted using a Bio-Rad microplate absorbance reader.

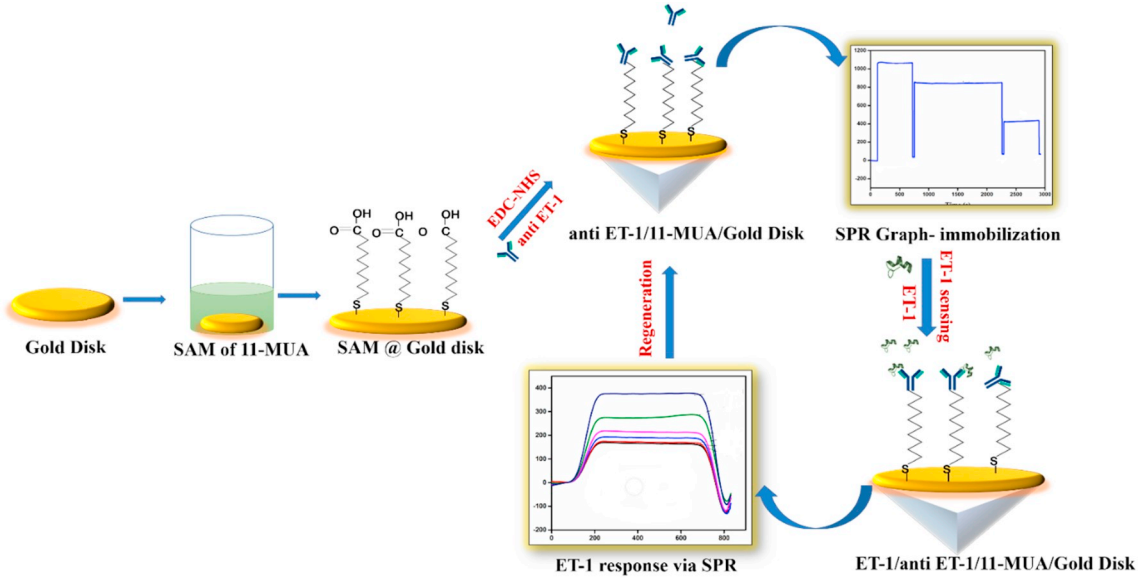

Scheme 1. Schematic illustration of gold disk modification for SPR biosensing.

3. Results and discussion

3.1. Optimization of anti-ET-1 concentration

The optimization of antibody concentration is a crucial step in the fabrication of a biosensor. In this study, the observed change in the response angle was obtained as a function of different concentration (50, 70, 100 and 150 μg mL^{-1}) of anti-ET-1 antibodies. The maximum change in angle was observed for 100 μg mL^{-1} of anti-ET-1 (Fig. 1A). However, at higher concentration (150 μg mL^{-1}) of anti-ET-1, the saturation of SPR angle occurred possibly because of steric hindrance. The observed saturation at 100 μg mL^{-1} was attributed to the complete immobilization of anti-ET-1 onto the activated sites of the SAM surface. Thus, 100 μg mL^{-1} of monoclonal anti-ET-1 was chosen for the fabrication of immunosensor. Fig. 1B shows the plot obtained between the SPR response angle (m°) and time(s), which clearly reveals the binding of anti-ET-1 at each step. The immobilization curve shows a baseline for 11-MUA/Au with continuous buffer flow at 10 μL/min. Thereafter 35 μL of EDC-NHS was added to activate the carboxyl groups of 11-MUA/Au (curve b). Further injection of anti-ET-1 leading to electrostatic interaction and coupling of the ligand on 11-MUA/Au matrix is shown by curve c. Next, 1 M ethanolamine was used to deactivate unreacted NHS-esters and remove electrostatically bound ligands (curve d) followed by baseline curve e. The change in the baseline toward the higher value indicated the modification of 11-MUA/Au disk with the linker (EDC-NHS) and anti-ET-1 antibodies. This could be assigned to the change in the refractive indices at each step of modification.

3.2. Fourier transform infrared spectroscopy studies

FT-IR spectroscopic studies were conducted in the 4000-500 cm^{-1} range to investigate the presence of functional groups or intermolecular binding occurring onto the (A) Au disk (B) 11-MUA/Au disk, and (C) anti-ET-1/11-MUA/Au disk (Fig. 2). The sharp peak at 1697 cm^{-1}

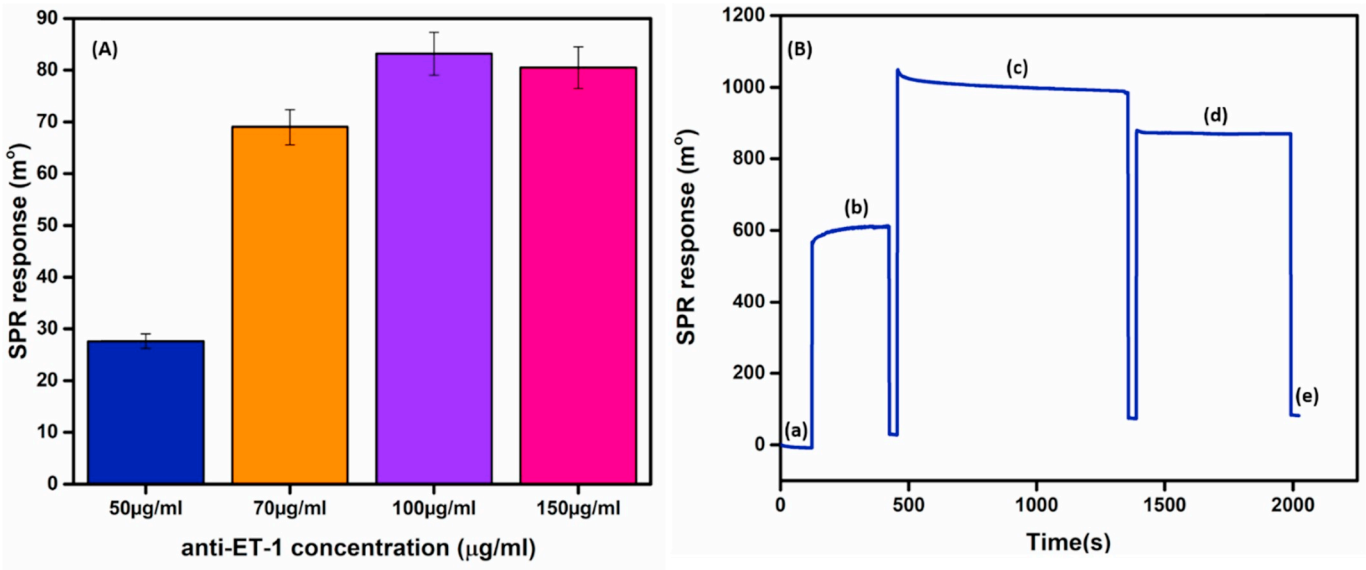

Fig. 1. (A) Optimization of anti-ET-1 immobilization using different concentration of 50 μg mL^{-1}, 70 μg mL^{-1},100 μg $mL^{-1}$and 150 μg mL^{-1}(difference in baseline obtained before immobilization and baseline after ethanolamine deactivation) (B) Immobilization of anti-ET-1 (a) Baseline of 11-MUA/Au, (b) EDC-NHS activation on 11-MUA/Au and (c) anti-ET-1/11-MUA/Au (d) ethanolamine deactivation (e) baseline.

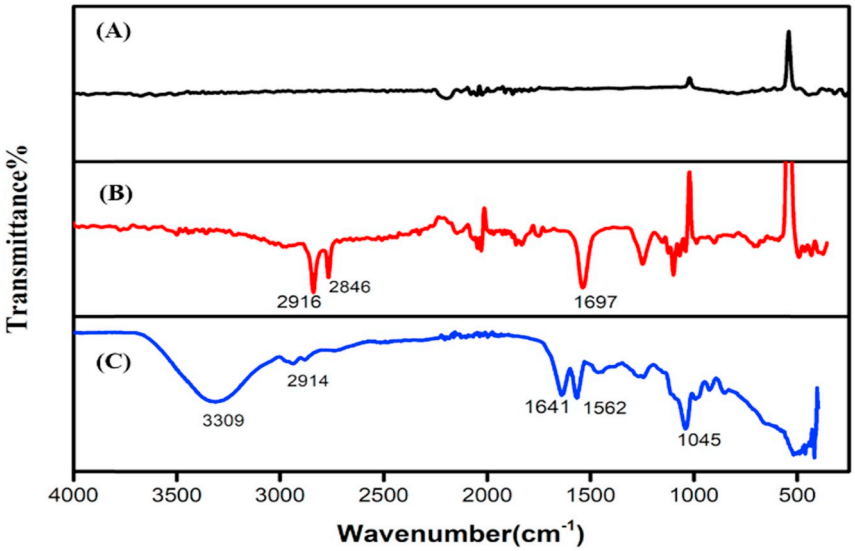

Fig. 2. FTIR spectra of (A) Au Disk, (B) 11-MUA/Au disk, (C) anti-ET-1/11-MUA/Au disk.

observed in the IR spectra (Fig. 2B) indicated the presence of –COOH groups of 11-MUA molecules confirming the formation of the 11-MUA SAM on the Au Disk (Fig. 2B). The other peaks are seen at 2916, and 2846 cm^{-1} corresponding to the stretching vibration of saturated $–CH_3$ groups further revealed the formation of 11-MUA layer onto the gold surface [42]. After anti-ET-1 immobilization the characteristic peaks obtained at 1641 and 1562 cm^{-1} were assigned to the presence of amide-I and amide-II bonds formed between the –COOH group of SAM and $–NH_2$ group of ET-1 antibody (Fig. 2C). The other peaks found at 3309 cm^{-1} and 1045 cm^{-1} were attributed to the presence of −OH and C−OH stretching vibrations of antibodies [43], respectively. These results confirmed the successful immobilization of anti-ET-1 with 11-MUA of the SAM layer on the gold disk.

3.3. Contact angle studies

To investigate the hydrophilic/hydrophobic properties of the modified Au disks, contact angle (CA) studies were conducted (Fig. 3A & B). After the 11-MUA SAM formation (Fig. 3A), the CA value was found to be 53.6° indicating increased hydrophilicity due to free –COOH groups introduced on to the Au disk. Interestingly, the CA angle decreased to 31.3° after anti-ET-1 immobilization (Fig. 3B). This increase in hydrophilicity was due to the hydrophilic nature of antibodies indicating the immobilization of anti-ET-1 onto the 11-MUA/Au electrode [44].

3.4. Atomic force microscopic studies

The atomic force microscopic (AFM) studies were conducted to investigate the changes in the surface morphology of the fabricated electrode. The average surface roughness of the gold disk modified with 11-MUA was found to be ~4.1 nm (Fig. 3C), confirming the smooth, dense and uniform SAM formation onto the Au disk. After the anti-ET-1 immobilization onto the 11-MUA/Au disk, the average roughness increased to ~9.8 nm (Fig. 3D) due to the globular structure of the antibodies that further covered the smooth surface of the SAM/Au disk [45]. The results of the AFM studies indicated the successful formation of the SAM onto the Au disk and the immobilization of anti-ET-1 biomolecules and were in agreement with the FT-IR studies.

3.5. Binding, response and kinetic analysis of ET-1

The SPR measurements were conducted to gain insight of the binding kinetics and biomolecular interactions of this novel biomarker (ET-1). This technique was used to investigate the binding response of the fabricated immunoelectrode as a function of ET-1 concentration. In SPR, the surface plasmon wave is generated and propagated along the boundary of metal and the dielectric. The propagation constant of the surface plasmon wave can be expressed as (Eq. (1))

$$\beta = \frac{\omega}{c}\sqrt{\frac{\varepsilon_M \varepsilon_D}{\varepsilon_M + \varepsilon_D}} \quad (1)$$

where ω is the angular frequency, εM and εD are the dielectric functions of metal and dielectric, respectively, and c is the speed of light. The change in the refractive index of the dielectric medium as a function of concentration resulted in a change in the intensity of surface plasmon wave that in turn led to the change in the SPR angle.

Fig. 4A shows the change in the SPR reflectance curve obtained at different concentrations of ET-1 as a function of time at room temperature (298 K). It was found that the shift in the curve was directly proportional to the increase in ET-1 concentration. Further, a calibration curve was plotted (Fig. S-1 A) between the change in SPR response in equilibrium versus ET-1 concentration (2–100 pg mL^{-1}). The change in R_{eq} with increasing concentration was found to be linear in the range, 2–100 pg mL^{-1} with an R^2 value of 0.99 and follows Eq. (2).

$$y = 2.18\,x + 165.05 \quad (2)$$

where *y* represents the change in SPR angle (Δm^o), and x represents the ET-1 concentration. Further, the sensitivity of the immunosensor was evaluated by using the slope of the curve and was found to be 2.18 m^o pg^{-1} mL, and the limit of detection (LOD) was calculated to be 0.30 pg mL^{-1} using Eq. (3).

$$\text{Limit of detection} = 3\sigma/\text{sensitivity} \quad (3)$$

where σ is the standard deviation of intercept. The shift observed in the SPR dip angle with increasing concentration of ET-1 (Fig. 4A) revealed that the refractive index changed along with the change in the surface density. Further, electrochemical impedance spectroscopy (EIS) studies were performed to investigate the dynamics of the antibody and antigen interaction occurring at the EA/anti-ET-1/11-MUA/Au electrode interface. In EIS, the Randles circuit is used for modelling the EIS data which consists of the capacitance of dielectric layer (C_{dl}), Warburg impedance (Z_w), and charge transfer resistance (R_{ct}) in series with electrolyte resistance (R_s). The typical Nyquist plot has a semicircle region which indicates the charge transfer limited process followed by a linear region revealing the mass transfer process. Fig. S-3 shows the Nyquist plot of (a) bare Au electrode, (b) 11-MUA/Au and (c) EA/anti-

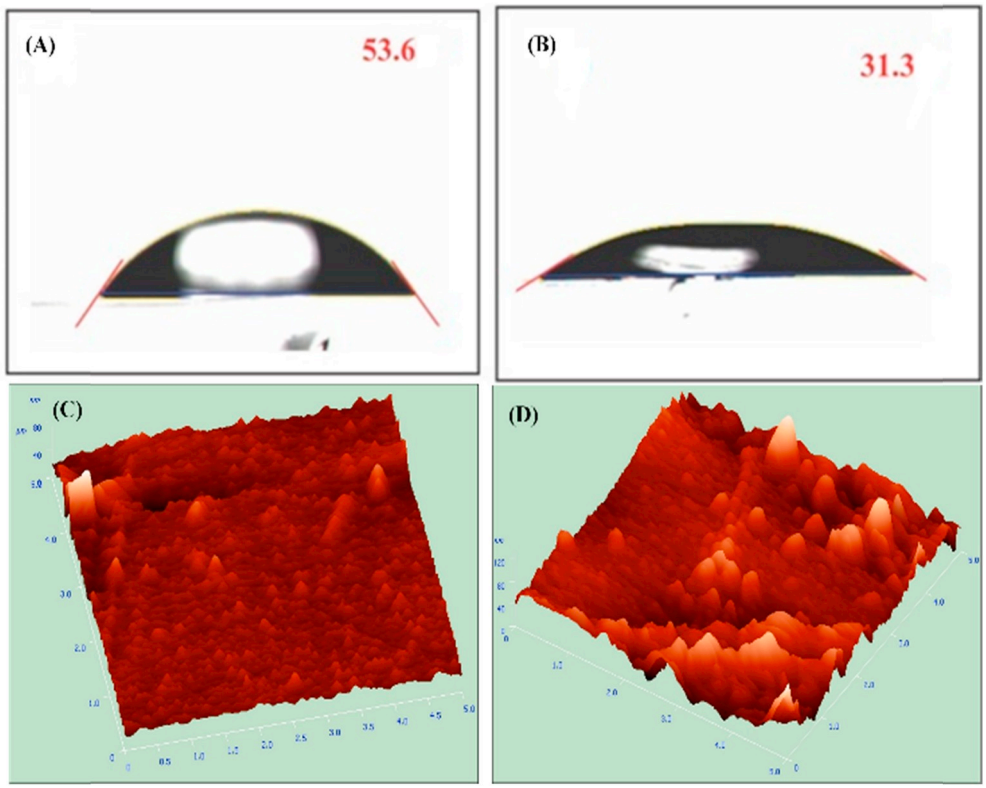

Fig. 3. Contact angle studies of (A) 11-MUA/Au electrode and (B) anti-ET-1/11-MUA/Au electrode. AFM micrographs of (C) 11-MUA/Au electrode and (D) anti-ET-1/11-MUA/Au electrode.

ET-1/11-MUA/Au electrode in PBS (pH-7.4) containing 5 mM $[Fe(CN)_6]^{4-/3-}$ in the frequency range, 10^5-0.1 Hz at a potential of 10 mV. The electron transfer resistance (R_{ct}) values for the bare gold, SAM-modified and antibody immobilized electrode were found to be 17.1 Ω, 1.33 kΩ, and 8.78 kΩ, respectively. The change in R_{ct} values with modification of the film indicated increased insulating characteristics of the SAM. The increased R_{ct} value after antibody immobilization was attributed to the insulating nature of the biomolecules that hindered the electron transport from bulk to the electrode surface. The heterogeneous electron transfer rate (k°) for bare Au, 11-MUA/Au, and EA/anti-ET-1/11-MUA/Au electrodes were calculated using Eq. (4).

$$k^{\circ} = RT/n^2F^2AR_{ct}C \quad (4)$$

where T is the temperature (~298 K), R is the molar gas constant, n is the number of electrons, C is the concentration of electroactive species (5×10^{-3} M), and A is the active surface area of the electrode (0.25 cm^2). The k° values of the bare Au, 11-MUA/Au, and EA/anti-ET-1/11-MUA/Au were determined to be 0.17 cm s^{-1}, 2.2×10^{-3} cm s^{-1} and 3.4×10^{-4} cm s^{-1}, respectively. Further, the impedimetric response of EA/anti-ET-1/11-MUA/Au as a function of the different

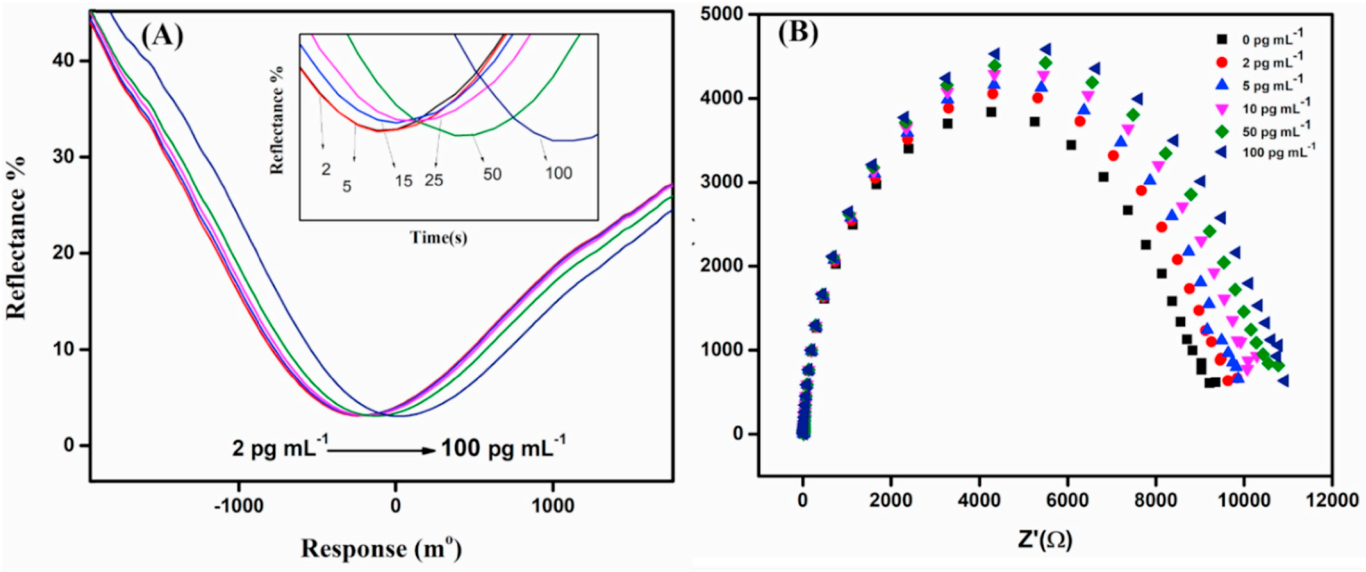

Fig. 4. Sensing response obtained for anti-ET-1 immobilized electrode exposed to different concentration of ET-1 (2–100 pg mL^{-1}) (A) SPR reflectance curve, (B) Impedance spectra.

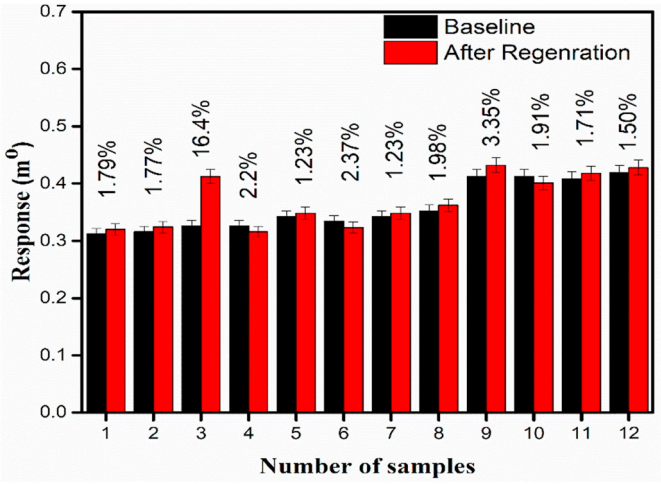

Fig. 5. Bar graph depicting the change in response angle of baseline after regeneration of immunosensor with the concentration of 5 pg mL^{-1}.

concentration of ET-1 (2–100 pg mL^{-1}) was obtained from the Nyquist plot (Fig. 4B). As the concentration of ET-1 was increased, the attachment of antigens on the modified electrode increased resulting in increased R_{ct} arising due to the formation of insulating antigen-antibody complexes. The calibration plot between the R_{ct} and ET-1 concentration exhibited a linear behaviour in the range (2–100 pg mL^{-1}) (Fig. S-1 B). The detection limit was calculated to be 0.36 pg mL^{-1} using Eq. (3).

Further, the binding kinetics of ET-1 onto the immunosensor surface undergoes two phases i.e., association and dissociation phase with ka and kd as an association constant and dissociation constant, respectively. The interaction between the ligand (anti-ET-1) and the analyte (ET-1) resulted in the formation of immunocomplex at the SPR sensor disk (EA/anti-ET-1/11-MUA/Au). The kinetics involved in the immunocomplex formation was evaluated using the observed experimental data. The dissociation phase was followed by the regeneration phase to reuse the electrode. The association constant of the analyte binding with the ligand was determined by a non-linear curve fitting using the SPR kinetic evaluation software. (Fig. S-2). Further, a monophasic model was assumed where the binding of the analyte at the sensor surface was considered to be in the ratio of 1:1 and was a single step process represented using the integrated rate equation (Rt) [46] involved during the association phase (Eq. (5)).

$$R_t = \frac{k_a C R_{max}}{k_a C + k_d}\left(1 - e^{-(k_a C + k_d)t}\right) + R_o \quad (5)$$

where C is the amount of ET-1 bound on the surface R_o is the response of signal at zero seconds, $k_a C\, R_{max}/k_a C + k_d$ is the maximal change in the binding response. The values of k_a and k_d were determined to be $4.4 \pm 0.4 \times 10^5\ M^{-1}\ s^{-1}$, and $2.04 \pm 0.0003 \times 10^{-3}\ s^{-1}$, respectively. Thus, the equilibrium constant K_A ($= k_a/k_d$) for association was obtained as $K_A = 2.15 \times 10^8\ M^{-1}$. The advantage of SPR immunosensor over the conventional techniques such as ELISA is reusability of the sensor surface. During the regeneration phase, the antigen is removed from the antibody while maintaining the functionality and reusability of the antibody at the sensor surface. Here, we observed the negligible difference in the SPR signal obtained before antigen sensing and after regeneration stage revealing successful recovery of the active surface of the immunoelectrode. This could perhaps be attributed to the fact that at low pH the protein binding sites tended to fold and repel each other making the molecules move apart. The % change in response to baseline after regeneration of the sensor surface is shown in Fig. 5. It was observed that the sensor could be regenerated more than ten times (~% RSD = 2.5).

Table 1
Characteristics of the 11-MUA based SPR biosensor along with those reported in the literature for colorectal cancer detection.

Method	Detection technique	Biosensing platform	Sample	Target Analyte	Label used	Degree of invasiveness	Range	Limit of detection (LOD)	Sensitivity	Reference
Colonoscopy	Visual Imaging	–	Tissue	–	–	High	–	–	–	[1]
Sigmoidoscopy	Visual Imaging	–	Tissue	–	–	High	–	–	–	[1]
Double Contrast barium enema	X-Ray Imaging	–	Tissue	–	–	High	–	–	–	[1]
Biosensor	SPR	Gold/ZnO nanocomposite	Serum	CA 15–3	No	Low	1–40 U mL^{-1}	0.0125 U ml^{-1}	–	[47]
	LSPR	Gold/MHDA/TAA	Serum	GTF2b and EDIL3	No	Low	50 ng mL^{-1} to 1 μg mL^{-1}	10 ngmL^{-1}and 5 ng mL^{-1}	–	[48]
	SPRi	OEG and COOH–OEG SAM Layer	Serum	CEA	No	Low	–	–	–	[49]
	SPRi	Gold/DNA probe H1	Serum	miRNA-15a	Yes	Low	0.5-5 fM	0.56 fM	–	[50]
	LSPR	Mixed PEG/GNR	Serum	ALCAM	No	Low	0.05 nM–25 nM	15 pM		[51]
	SPR	Gold/MUA	Serum	ET-1	No	Low	2 pg mL^{-1}-100 pg mL^{-1}	0.30 pgmL^{-1}	2.38 m° pg^{-1} mL	This work

3.5.1. Non-specific interaction and interferent studies

Reducing non-specific interaction is crucial as it helps to obtain good binding curves. To reduce nonspecific interaction on the SPR sensor surface, we introduced salts such as NaCl (0.138 M), KCl (0.027 M) and tween 20 into the running buffer as it reduces the charge interactions by shielding effect. Moreover, we also used ethanolamine (EA) to reduce the interaction of other proteins on the sensor surface and on the attached ligand. To evaluate the specificity of this SPR immunosensor towards ET-1, interferent studies were conducted. In serum samples of cancer patients, several biological molecules such as glucose (100 mg dL^{-1}), cardiac troponin I (cTnI 0.40 ng mL^{-1}), cytokeratin 19 fragments (CYFRA-21-1 3.5 ng mL^{-1}), and carcinoembryonic antigen (CEA 3 ng mL^{-1}) are known to be present and are potential interferents. The fabricated SPR sensor disk was subjected to these different interferents starting with ET-1 followed by incorporation of cTnI, CYFRA-21-1, CEA and glucose. The obtained SPR response angle did not exhibit any significant change when subjected to various interferents (Fig. S-4), revealing high specificity of the immunosensor to ET-1. Table 1 shows the characteristics of this ET-1 SPR immunosensor along with those reported in the literature for colorectal cancer detection.

3.6. Serum sample analysis

A study was conducted to assess the applicability of the fabricated SPR immunosensor towards the serum samples taken from CRC patients. These results were validated against those obtained by ELISA (Table 2). The detailed procedures of sample collection and analysis by SPR and ELISA have been provided in the supplementary data Section 1.1 and 1.2.

Fig. S-5 shows the bar graph representation comparing the change in response angle with respect to the patient samples and standard samples with an acceptable %RSD (0.63–1.64). The LOD for the serum sample was calculated to be 4.6 pg mL^{-1}. The small deviation in sensitivity of serum samples with respect to the standard samples may perhaps be due to other interfering compounds present in natural serum samples of the patients. This SPR based detection was found to be more sensitive, less time consuming and exhibited a better LOD than ELISA kit. The results obtained using this SPR immunosensor, ELISA and EIS towards the determination of ET-1 levels have been tabulated in Table 3.

4. Conclusions

In this study, a simple, label-free SPR immunosensor has been fabricated for real-time detection of ET-1, a colorectal cancer biomarker for the first time. The SPR Au sensor disk has been initially modified with SAM (11-MUA) followed by immobilization of anti-ET-1 and EA. This ET-1 based SPR sensor disk has been characterized via contact angle, FT-IR, and AFM techniques. The interaction mechanism of antigen (ET-1) and antibody (anti-ET1) was evaluated by different model amongst which the monophasic model revealed better results. The

Table 2
Determination of ET-1 concentration in the serum sample of colorectal patients by ELISA technique and EA/anti-ET-1/11-MUA/Au SPR immunosensor.

Patient sample	Concentration of ET-1 in serum sample determined from ELISA (pg mL^{-1})	Concentration of ET-1 in serum sample determined by developed SPR disk (pg mL^{-1})	%RSD (n = 3)
1	9.4	9.7	2.22
2	10.3	10.04	1.81
3	10.5	10.21	1.98
4	10.9	10.3	4.0
5	11.5	11.2	1.87
6	15	15.4	1.86

Table 3
Comparison between different techniques used in this study to determine the presence of ET-1.

Techniques	Linear range (pg mL^{-1})	LOD (pg mL^{-1})	Advantages	Limitations	Ref.
RayBio Human Endothelin-1 ELISA Kit	10–1000	10	Gold standard technique Specific and sensitive	Time-consuming, Labor intensive	[52]
SPR	2–100	0.30	Real-time monitoring, Kinetic studies, label-free, sensitive	Plasmon effect limited to gold or silver surface.	Present study
EIS	2–100	0.36	Highly Sensitive, Miniaturization possible	Kinetic interaction cannot be studied, no real-time interaction monitoring,	

linear range of this sensor has been found to be 2–100 pg mL^{-1} with a LOD of 0.36 pg mL^{-1} and a remarkable sensitivity of 2.18 m^{o} pg^{-1} mL. Real-time analysis of the serum sample obtained using this SPR sensor has been compared with ELISA and electrochemical impedance spectroscopy results. The fabricated biosensor shows remarkable sensitivity, selectivity, and reproducibility in real time sensing of ET-1. The excellent performance of SPR biosensor for ET-1 detection as a potential biomarker for CRC detection paves the way for effective diagnosing method towards cancer detection as compared to conventional methods. Further efforts should also be made to fabricate a portable SPR biosensor for point-of-care diagnostics.

Acknowledgements

We thank Prof. Yogesh Singh, Vice Chancellor, Delhi Technological University (DTU), Delhi, India for providing the facilities. TN is thankful to DBT, India (BT/PR12530/MED/32/385/2015) for providing financial assistance. BDM thanks Science & Engineering Research Board (Govt. of India) for the award of a Distinguished Fellowship (SB/S9/YSCP/SERB-DF/2018(1)). Saurabh Kumar and Suveen Kumar acknowledge Department of Science and Technology, New Delhi, India for DST INSPIRE Faculty Award (DST/INSPIRE/04/2017/002750 and DST/INSPIRE/04/2017/001336, respectively).

Appendix A. Supplementary data

Supplementary data to this article can be found online at https://doi.org/10.1016/j.talanta.2019.04.039.

References

[1] R.L. Siegel, K.D. Miller, S.A. Fedewa, D.J. Ahnen, R.G. Meester, A. Barzi, A. Jemal, Colorectal cancer statistics, 2017, Ca - Cancer J. Clin. 67 (3) (2017) 177–193.
[2] L.A. Torre, F. Bray, R.L. Siegel, J. Ferlay, J. Lortet-Tieulent, A. Jemal, Global cancer statistics, Ca - Cancer J. Clin. 65 (2) (2012) 87–108 2015.
[3] C. Allemani, H.K. Weir, H. Carreira, R. Harewood, D. Spika, X.-S. Wang, F. Bannon, J.V. Ahn, C.J. Johnson, A. Bonaventure, Global surveillance of cancer survival 1995–2009: analysis of individual data for 25 676 887 patients from 279 population-based registries in 67 countries (CONCORD-2), Lancet 385 (9972) (2015) 977–1010.
[4] A. Jemal, R. Siegel, J. Xu, E. Ward, Cancer statistics, Ca - Cancer J. Clin. 60 (5) (2010) 277–300 2010.
[5] A. Ekbom, C. Helmick, M. Zack, H.-O. Adami, Ulcerative colitis and colorectal cancer: a population-based study, N. Engl. J. Med. 323 (18) (1990) 1228–1233.
[6] M.G. Collins, E. Teo, S.R. Cole, C.-Y. Chan, S.P. McDonald, G.R. Russ, G.P. Young, P.A. Bampton, P.T. Coates, Screening for colorectal cancer and advanced colorectal neoplasia in kidney transplant recipients: cross sectional prevalence and diagnostic accuracy study of faecal immunochemical testing for haemoglobin and colonoscopy, BMJ 345 (2012) e4657.
[7] E. Giovannucci, Insulin and colon cancer, Cancer Causes Control 6 (2) (1995) 164–179.
[8] H. Yuhara, C. Steinmaus, S.E. Cohen, D.A. Corley, Y. Tei, P.A. Buffler, Is diabetes mellitus an independent risk factor for colon cancer and rectal cancer? Am. J. Gastroenterol. 106 (11) (2011) 1911–1921.
[9] E. Cho, J.E. Lee, E.B. Rimm, C.S. Fuchs, E.L. Giovannucci, Alcohol consumption and the risk of colon cancer by family history of colorectal cancer, Am. J. Clin. Nutr. 95 (2) (2012) 413–419.
[10] Y. Kimura, S. Kono, K. Toyomura, J. Nagano, T. Mizoue, M.A. Moore, R. Mibu, M. Tanaka, Y. Kakeji, Y. Maehara, Meat, fish and fat intake in relation to subsite-specific risk of colorectal cancer: the Fukuoka colorectal cancer study, Cancer Sci. 98 (4) (2007) 590–597.
[11] D. Harriss, G. Atkinson, A. Batterham, K. George, N. Tim Cable, T. Reilly, N. Haboubi, A.G. Renehan, Lifestyle factors and colorectal cancer risk (2): a systematic review and meta-analysis of associations with leisure-time physical activity, Colorectal Dis. 11 (7) (2009) 689–701.
[12] B. Ji, Q. Dai, Y. Gao, A. Hsing, J. McLaughlin, J. Fraumeni Jr., W. Chow, Cigarette and alcohol consumption and the risk of colorectal cancer in Shanghai, China, Eur. J. Cancer Prev. 11 (3) (2002) 237–244.
[13] P. Thirunavukarasu, S. Sukumar, M. Sathaiah, M. Mahan, K.D. Pragatheeshwar, J.F. Pingpank, H. Zeh, C.J. Bartels, K.K. Lee, D.L. Bartlett, C-stage in colon cancer: implications of carcinoembryonic antigen biomarker in staging, prognosis, and management, JNCI: J. Natl. Cancer Inst. 103 (8) (2011) 689–697.
[14] P.J. Pickhardt, C. Hassan, S. Halligan, R. Marmo, Colorectal cancer: CT colonography and colonoscopy for detection—systematic review and meta-analysis, Radiology 259 (2) (2011) 393–405.
[15] N. Wasserberg, O. Purim, V. Bard, Y. Kundel, N. Gordon, D. Groshar, N. Goldberg, H. Kashtan, A. Sulkes, B. Brenner, Early postoperative 18F-FDG PET/CT in high-risk stage III colorectal cancer, Clin. Nucl. Med. 40 (4) (2015) e222–e227.
[16] F. Tixier, A.M. Groves, V. Goh, M. Hatt, P. Ingrand, C.C. Le Rest, D. Visvikis, Correlation of intra-tumor 18F-FDG uptake heterogeneity indices with perfusion CT derived parameters in colorectal cancer, PLoS One 9 (6) (2014) e99567.
[17] H.J. Wanebo, B. Rao, C.M. Pinsky, R.G. Hoffman, M. Stearns, M.K. Schwartz, H.F. Oettgen, Preoperative carcinoembryonic antigen level as a prognostic indicator in colorectal cancer, N. Engl. J. Med. 299 (9) (1978) 448–451.
[18] P. Byström, Colorectal Cancer Treatment and Early Response Evaluation, How do We Best Evaluate Treatment Response?, Institutionen för Onkologi-Patologi/Department of Oncology-Pathology, (2010).
[19] W. Zhong, Z. Yu, J. Zhan, T. Yu, Y. Lin, Z.-S. Xia, Y.-H. Yuan, Q.-K. Chen, Association of serum levels of CEA, CA199, CA125, CYFRA21-1 and CA72-4 and disease characteristics in colorectal cancer, Pathol. Oncol. Res. 21 (1) (2015) 83–95.
[20] A. Nicolini, P. Ferrari, M.J. Duffy, A. Antonelli, G. Rossi, M.R. Metelli, F. Fulceri, L. Anselmi, M. Conte, P. Berti, Intensive risk-adjusted follow-up with the CEA, TPA, CA19. 9, and CA72. 4 tumor marker panel and abdominal ultrasonography to diagnose operable colorectal cancer recurrences: effect on survival, Arch. Surg. 145 (12) (2010) 1177–1183.
[21] Z. Huang, D. Huang, S. Ni, Z. Peng, W. Sheng, X. Du, Plasma microRNAs are promising novel biomarkers for early detection of colorectal cancer, Int. J. Cancer 127 (1) (2010) 118–126.
[22] K.-J. Feng, Y.-H. Yang, Z.-J. Wang, J.-H. Jiang, G.-L. Shen, R.-Q. Yu, A nano-porous CeO 2/Chitosan composite film as the immobilization matrix for colorectal cancer DNA sequence-selective electrochemical biosensor, Talanta 70 (3) (2006) 561–565.
[23] G.Y. Locker, S. Hamilton, J. Harris, J.M. Jessup, N. Kemeny, J.S. Macdonald, M.R. Somerfield, D.F. Hayes, R.C. Bast Jr., ASCO 2006 update of recommendations for the use of tumor markers in gastrointestinal cancer, J. Clin. Oncol. 24 (33) (2006) 5313–5327.
[24] M. Duffy, R. Lamerz, C. Haglund, A. Nicolini, M. Kalousová, L. Holubec, C. Sturgeon, Tumor markers in colorectal cancer, gastric cancer and gastrointestinal stromal cancers: european group on tumor markers 2014 guidelines update, Int. J. Cancer 134 (11) (2014) 2513–2522.
[25] F. Lumachi, F. Marino, R. Orlando, G.B. Chiara, S.M. Basso, Simultaneous multianalyte immunoassay measurement of five serum tumor markers in the detection of colorectal cancer, Anticancer Res. 32 (3) (2012) 985–988.
[26] L. Tao, K. Zhang, Y. Sun, B. Jin, Z. Zhang, K. Yang, Anti-epithelial cell adhesion molecule monoclonal antibody conjugated fluorescent nanoparticle biosensor for sensitive detection of colon cancer cells, Biosens. Bioelectron. 35 (1) (2012) 186–192.
[27] M. Yanagisawa, H. Kurihara, S. Kimura, Y. Tomobe, M. Kobayashi, Y. Mitsui, Y. Yazaki, K. Goto, T. Masaki, A novel potent vasoconstrictor peptide produced by vascular endothelial cells, Nature 332 (6163) (1988) 411–415.
[28] I.A. Abdel-Gawad, H. Hassanein, N.A. Bahgat, M. Abdel Sattar, A.H. El-Sissy, M.A. Altaweel, A.M. Helal, Study of endothelin-1 and vascular endothelial growth factor in patients with cancer colon, J. Egypt. Natl. Cancer Inst. 20 (3) (2008) 216–223.
[29] H. Inagaki, A.E. Bishop, T. Eimoto, J.M. Polak, Autoradiographic localization of endothelin-1 binding sites in human colonic cancer tissue, J. Pathol. 168 (3) (1992) 263–267.
[30] M. Shichiri, Y. Hirata, T. Nakajima, K. Ando, T. Imai, M. Yanagisawa, T. Masaki, F. Marumo, Endothelin-1 is an autocrine/paracrine growth factor for human cancer cell lines, J. Clin. Investig. 87 (5) (1991) 1867.
[31] A. Bagnato, R. Tecce, V. Di Castro, K.J. Catt, Activation of mitogenic signaling by endothelin 1 in ovarian carcinoma cells, Cancer Res. 57 (7) (1997) 1306–1311.
[32] S. Moraitis, S. Langdon, W. Miller, Endothelin expression and responsiveness in human ovarian carcinoma cell lines, Eur. J. Cancer 33 (4) (1997) 661–668.
[33] E. Asham, A. Shankar, M. Loizidou, S. Fredericks, K. Miller, P. Boulos, G. Burnstock, I. Taylor, Increased endothelin-1 in colorectal cancer and reduction of tumour growth by ET, Br. J. Canc. 85 (11) (2001) 1759–1763.
[34] A. Shankar, M. Loizidou, G. Aliev, S. Fredericks, D. Holt, P. Boulos, G. Burnstock, I. Taylor, Raised endothelin 1 levels in patients with colorectal liver metastases, Br. J. Surg. 85 (4) (1998) 502–506.
[35] J. Knowles, M. Loizidou, Irving Taylor, Endothelin-1 and angiogenesis in cancer, Curr. Vasc. Pharmacol. 3 (4) (2005) 309–314.
[36] J. León, J. Casado, S.M. Jiménez Ruiz, M.S. Zurita, C. González-Puga, J.D. Rejón, A. Gila, P. Muñoz de Rueda, E.J. Pavón, Russel J. Reiter, Angela Ruiz-Extremera, Javier Salmerón, Melatonin reduces endothelin-1 expression and secretion in colon cancer cells through the inactivation of FoxO-1 and NF-κβ, J. Pineal Res. 56 (4) (2014) 415–426.
[37] R. Cianfrocca, L. Rosanò, P. Tocci, R. Sestito, V. Caprara, V. Di Castro, R. De Maria, A. Bagnato, Blocking endothelin-1-receptor/β-catenin circuit sensitizes to chemotherapy in colorectal cancer, Cell Death Differ. 24 (2017) 1811.
[38] H. Ali, M. Loizidou, M. Dashwood, F. Savage, C. Sheard, I. Taylor, Stimulation of colorectal cancer cell line growth by ET-1 and its inhibition by ET A antagonists, Gut 47 (5) (2000) 685–688.
[39] Z. Matharu, A.J. Bandodkar, G. Sumana, P.R. Solanki, E.M. Ekanayake, K. Kaneto, V. Gupta, B. Malhotra, Low density lipoprotein detection based on antibody immobilized self-assembled monolayer: investigations of kinetic and thermodynamic properties, J. Phys. Chem. B 113 (43) (2009) 14405–14412.
[40] B.D. Malhotra, M.A. Ali, Nanomaterials for Biosensors: Fundamentals and Applications, William Andrew, 2017.
[41] M. Corr, A.E. Slanetz, L.F. Boyd, M.T. Jelonek, S. Khilko, B.K. Al-Ramadi, Y.S. Kim, S.E. Maher, A.L. Bothwell, D.H. Margulies, T Cell Receptor-MHC Class I Peptide Interactions: Affinity, Kinetics, and Specificity, Science-New York then Washington, 1994 946-946.

[42] R. Zhu, J. Song, Q. Ma, Y. Zhou, J. Yang, S. Shuang, C. Dong, A colorimetric probe for the detection of aluminum ions based on 11-mercaptoundecanoic acid functionalized gold nanoparticles, Anal. Methods 8 (39) (2016) 7232–7236.
[43] I. Tubía, J. Paredes, E. Pérez-Lorenzo, S. Arana, Antibody biosensors for spoilage yeast detection based on impedance spectroscopy, Biosens. Bioelectron. 102 (2018) 432–438.
[44] S. Kumar, J. Singh, V. Agrawal, M. Ahamad, B.J.A.M. Malhotra, Biocompatible self-assembled monolayer platform based on (3-glycidoxypropyl) trimethoxysilane for total cholesterol estimation, 3 (10) (2011) 2237–2245.
[45] S. Kumar, S. Kumar, S. Tiwari, S. Augustine, S. Srivastava, B.K. Yadav, B.D. Malhotra, Highly sensitive protein functionalized nanostructured hafnium oxide based biosensing platform for non-invasive oral cancer detection, Sensor. Actuator. B Chem. 235 (2016) 1–10.
[46] R.B. Schasfoort, Handbook of Surface Plasmon Resonance, Royal Society of Chemistry, 2017.
[47] C.-C. Chang, N.-F. Chiu, D.S. Lin, Y. Chu-Su, Y.-H. Liang, C.-W. Lin, High-sensitivity detection of carbohydrate antigen 15-3 using a gold/zinc oxide thin film surface plasmon resonance-based biosensor, Anal. Chem. 82 (4) (2010) 1207–1212.
[48] M. Soler, M.-C. Estevez, R. Villar-Vazquez, J.I. Casal, L.M. Lechuga, Label-free nanoplasmonic sensing of tumor-associate autoantibodies for early diagnosis of colorectal cancer, Anal. Chim. Acta 930 (2016) 31–38.
[49] J. Ladd, H. Lu, A.D. Taylor, V. Goodell, M.L. Disis, S. Jiang, Direct detection of carcinoembryonic antigen autoantibodies in clinical human serum samples using a surface plasmon resonance sensor, Colloids Surfaces B Biointerfaces 70 (1) (2009) 1–6.
[50] F. Hu, J. Xu, Y. Chen, Surface plasmon resonance imaging detection of sub-femtomolar MicroRNA, Anal. Chem. 89 (18) (2017) 10071–10077.
[51] J.-H. Pai, C.-T. Yang, H.-Y. Hsu, A.B. Wedding, B. Thierry, Development of a simplified approach for the fabrication of localised surface plasmon resonance sensors based on gold nanorods functionalized using mixed polyethylene glycol layers, Anal. Chim. Acta 974 (2017) 87–92.
[52] Raybiotech, Human Endothelin-1 ELISA, (2019) https://www.raybiotech.com/human-endothelin-1-elisa/.